Radiotherapy and Oncology 134 (2019) 158–165

Contents lists available at ScienceDirect

Radiotherapy and Oncology

journal homepage: www.thegreenjournal.com

Original Article

In-vivo treatment accuracy analysis of active motion-compensated liver SBRT through registration of plan dose to post-therapeutic MRI-morphologic alterations

Judit Boda-Heggemann [a,*], Anika Jahnke [a,*], Mark K.H. Chan [b], Floris Ernst [c], Ardekani Leila Ghaderi [b], Ulrike Attenberger [d], Peter Hunold [e], Jost Philipp Schäfer [f], Stefan Wurster [g,h], Dirk Rades [i], Guido Hildebrandt [j], Frank Lohr [k], Jürgen Dunst [b], Frederik Wenz [a], Oliver Blanck [b,g]

[a] *Department of Radiation Oncology, Universitätsmedizin Mannheim, Medical Faculty Mannheim, Heidelberg University, Mannheim;* [b] *University Medical Center Schleswig-Holstein, Department of Radiation Oncology, Kiel;* [c] *University of Lübeck, Institute for Robotic and Cognitive Systems, Lübeck;* [d] *IKRN, Universitätsmedizin Mannheim, Medical Faculty Mannheim, Heidelberg University, Mannheim;* [e] *University Medical Center Schleswig-Holstein, Department of Radiology and Nuclear Medicine, Lübeck;* [f] *University Medical Center Schleswig-Holstein, Department of Radiology and Neuroradiology, Kiel;* [g] *Saphir Radiosurgery Center, Güstrow;* [h] *University Medicine Greifswald, Ambulatory Healthcare Center, Department of Radiation Oncology, Greifswald;* [i] *University Medical Center Schleswig-Holstein, Department of Radiation Oncology, Lübeck;* [j] *University Medicine Rostock, Department of Radiation Oncology, Rostock, Germany;* [k] *UO di Radioterapia, Dipartimento di Oncologia, Azienda Ospedaliero-Universitaria di Modena, Italy*

ARTICLE INFO

Article history:
Received 17 October 2018
Received in revised form 18 January 2019
Accepted 19 January 2019
Available online 15 February 2019

Keywords:
Gantry-based SBRT
Robotic SBRT
Normal tissue reactions
In-vivo accuracy
Active motion-management
DIBH

ABSTRACT

Background/purpose: *In-vivo*-accuracy analysis (IVA) of dose-delivery with active motion-management (gating/tracking) was performed based on registration of post-radiotherapeutic MRI-morphologic-alterations (MMA) to the corresponding dose-distributions of gantry-based/robotic SBRT-plans.

Methods: Forty targets in two patient cohorts were evaluated: (1) gantry-based SBRT (deep-inspiratory breath-hold-gating; GS) and (2) robotic SBRT (online fiducial-tracking; RS). The planning-CT was deformably registered to the first post-treatment contrast-enhanced T1-weighted MRI. An isodose-structure cropped to the liver (ISL) and corresponding to the contoured MMA was created. Structure and statistical analysis regarding volumes, surface-distance, conformity metrics and center-of-mass-differences (CoMD) was performed.

Results: Liver volume-reduction was −43.1 ± 148.2 cc post-RS and −55.8 ± 174.3 cc post-GS. The mean surface-distance between MMA and ISL was 2.3 ± 0.8 mm (RS) and 2.8 ± 1.1 mm (GS). ISL and MMA volumes diverged by 5.1 ± 23.3 cc (RS) and 16.5 ± 34.1 cc (GS); the median conformity index of both structures was 0.83 (RS) and 0.80 (GS). The average relative directional errors were ≤0.7 mm (RS) and ≤0.3 mm (GS); the median absolute 3D-CoMD was 3.8 mm (RS) and 4.2 mm (GS) without statistically significant differences between the two techniques. Factors influencing the IVA included GTV and PTV ($p = 0.041$ and $p = 0.020$). Four local relapses occurred without correlation to IVA.

Conclusions: For the first time a method for IVA was presented, which can serve as a benchmarking-tool for other treatment techniques. Both techniques have shown median deviations <5 mm of planned dose and MMA. However, IVA also revealed treatments with errors ≥5 mm, suggesting a necessity for patient-specific safety-margins. Nevertheless, the treatment accuracy of well-performed active motion-compensated liver SBRT seems not to be a driving factor for local treatment failure.

© 2019 Elsevier B.V. All rights reserved. Radiotherapy and Oncology 134 (2019) 158–165

Advanced motion-management techniques have the potential to increase local control and decrease toxicity of liver SBRT (stereotactic body radiotherapy [1–6]). Characteristic morphologic alterations in healthy liver tissue histologically corresponding to a veno-occlusive disease [7] have been observed in post-SBRT imaging [8,9,10–14]. If these alterations directly correspond to a clinical toxicity (transient liver enzyme-elevation/albumin-reduction [15,16]) is so far unknown. Symptomatic toxicity of SBRT for liver metastases is extremely low [2], however, plays a role for SBRT of primary liver tumors arising the basis of chronic liver damage [17,18]. Child-Pugh-B/C stage cirrhosis requires the adaption of

Abbreviations: IVA, *in-vivo*-accuracy analysis; MMA, MRI-morphologic-alterations; ISL, isodose-structure cropped to the liver; CoMD, center-of-mass-differences; GS, gantry-based SBRT; RS, robotic SBRT.

* Corresponding authors at: Department of Radiation Oncology, University Medical Center Mannheim, University of Heidelberg, Theodor-Kutzer Ufer 1-3, 68167 Mannheim, Germany.

E-mail address: judit.boda-heggemann@umm.de (J. Boda-Heggemann).

https://doi.org/10.1016/j.radonc.2019.01.023
0167-8140/© 2019 Elsevier B.V. All rights reserved.

the dose constraints [19], possibly compromising tumor control. Further examination of partial liver radiation tolerance based on imaging information is therefore of essential interest to define dose-constraints for each radiation application technique.

After gantry-based SBRT (GS) in DIBH (deep inspiration breath-hold) with additional ultrasound-based surveillance [20,21], threshold doses of nominally 20–21 Gy (equivalent dose in 2 Gy-fractions [EQD2] with $\alpha/\beta = 3$ Gy of 38–42 Gy_3) induced beam-path-like liver tissue changes that are clearly related to treatment technique characteristics [22]. For robotic SBRT (RS) with fiducial-based real-time target tracking [1,23], median nominal doses of 10.1–11.3 Gy per fraction (EQD2 79–97 Gy_3) induced centroid morphologic alterations surrounding the treated lesions [10]. The localizations of the sharply marked-off post-treatment morphologic alterations were found for both methods in the region surrounding the necrotic gross tumor volume (GTV). This fact indicates a reliable accuracy of SBRT with active motion-management. However, it was based on a descriptive presentation of the phenomenon of post-SBRT MRI alterations and their respective patient/treatment parameter impact and a registration to the treatment plan and quantification of the accuracy has never been performed.

In this work, we developed a new method for assessing the dose delivery accuracy based on registration of the dose-distribution to post-therapeutic MRI-morphologic alterations (MMA) and quantification of the geometrical and spatial properties of the dose cloud and the MMA.

Post-therapeutic MMA were contoured and registered to the corresponding isodose structure cropped to the liver (ISL) of gantry-based or robotic SBRT plans. Based on this registration, *in-vivo*-accuracy analysis (IVA) of dose delivery with active motion-management (gating/tracking) was performed by structure-analysis regarding volumes, surface distance and conformity metrics and center-of-mass differences (CoMD) for ISL and MMA. With that, we aimed at the systematic comparison of the accuracy of two delivery methods with advanced motion management (free-breathing treatment with fiducial tracking by CyberKnife versus linac-based breath-hold gating with additional ultrasound monitoring) with each other. All parameters were compared for both methods (GS and RS) and factors potentially influencing IVA were analyzed statistically.

Patients and methods

Patient characteristics

Two patient cohorts were evaluated retrospectively after approval by the local ethics committees of the medical faculty of the universities of Kiel (D458/17) and Mannheim (2014-413M-MA, amendment 2017, 2018-869R-MA).

1. Patients with gantry-based SBRT (GS) using the Versa-HD linear accelerator (Elekta AB, Stockholm, Sweden) with DIBH-based gating and ultrasound-surveillance of the gating [20,21] and
2. Patients with robotic SBRT (RS) using the CyberKnife (Accuray Inc, Sunnyvale, CA, USA) with real-time fiducial tracking during free breathing [1,23].

From each cohort, 20 planning target volumes (altogether 30 patients, 47 lesions and 37 plans) were analyzed. 3 plans included 2 PTVs due to geographic vicinity of the metastases. Patient characteristics (age, gender, Karnofsky-performance, primary tumor histology, prior treatment-schedules, chemotherapies and liver damage as well as GTV and planning target volume (PTV)-dimensions and applied doses) are summarized in Table 1.

Treatment planning and delivery

For all GS patients, the treatment planning CT was acquired in ABC®-based moderately deep inspiratory breath-hold (DIBH, Active Breathing Coordinator, Elekta AB) and contrast enhancement. GTV was defined based on a fusion with a liver-specific contrast enhanced planning MRI (VIBE sequence in voluntary DIBH). GTV-to-PTV-margins of radially 5 mm and craniocaudally 10 mm were applied. Flattening-filter-free VMAT-plans (Monaco vers. 5.11; Elekta AB) were created with 60 Gy in 5 fractions (12 Gy per fraction) prescribed to encompass 95% of the PTV. Daily inter-fractional imaging with breath-hold-only cone-beam-CT (Elekta AB; kV projections exclusively acquired during

Table 1
Patient and treatment characteristics. DIBH = deep inspiratory breath hold, HCC = hepatocellular carcinoma, CCC = cholangiocellular carcinoma, GTV = gross tumor volume, PTV = planning target volume, BED = biological equivalent dose, EQD2 = equivalent dose in 2 Gy fractions.

		Robotic SBRT (RS) with fiducial tracking	Gantry-based SBRT (GS) in DIBH
Patients (*n*)		14	16
Liver lesions (*n*)		24	23
Treatment plans (*n*)		17	20
Gender (*n*)	Male/Female	8/6	11/5
Age at treatment (years)	Median (range)	62 (34–83)	59 (45–83)
Karnofsky-Index (%)		90 (70–100)	95 (70–100)
Primary tumor (*n*)	Colorectal	7	5
based on patients	HCC/CCC	1	3
	Breast cancer	2	2
	Other	4	6
Treatments prior SBRT (*n*)	Liver surgery	13	7
based on series	Liver SBRT or Radiotherapy	5	5
	Chemotherapy	17	15
GTV (cc)	*based on lesions* Median (range)	18.9 (1.2–205.0)	9.5 (0.8–882)
Max GTV dimension (cm)		3 (1.3–7.3)	2 (1.3–36.5)
PTV (cc)		58 (9.0–318.0)	35 (8.5–1000.1)
Max PTV dimension (cm)		5 (2.6–8.5)	4 (2.7–96.1)
PTV prescription BED (Gy_{10})		90 (57–112.5)	132 (50.7–132)
GTV mean BED_{10Gy} (Gy_{10})		149 (88.3–170.1)	172 (46.4–218.1)
Total liver volume (cc)	*based on series*	1705 (1111–2135)	1644 (1147–2331)
Healthy liver volume (cc)	Median (range)	1700 (1062–1991)	1570 (1138–2330)
Mean total liver EQD2 (Gy_3)		18 (1.7–29.2)	7 (0.4–19.5)
Mean healthy liver EQD2 (Gy_3)		15 (1.5–24.7)	7 (0.4–18.6)
Time to MRI (weeks)		12 (7.3–16.9)	9 (6.1–20.3)

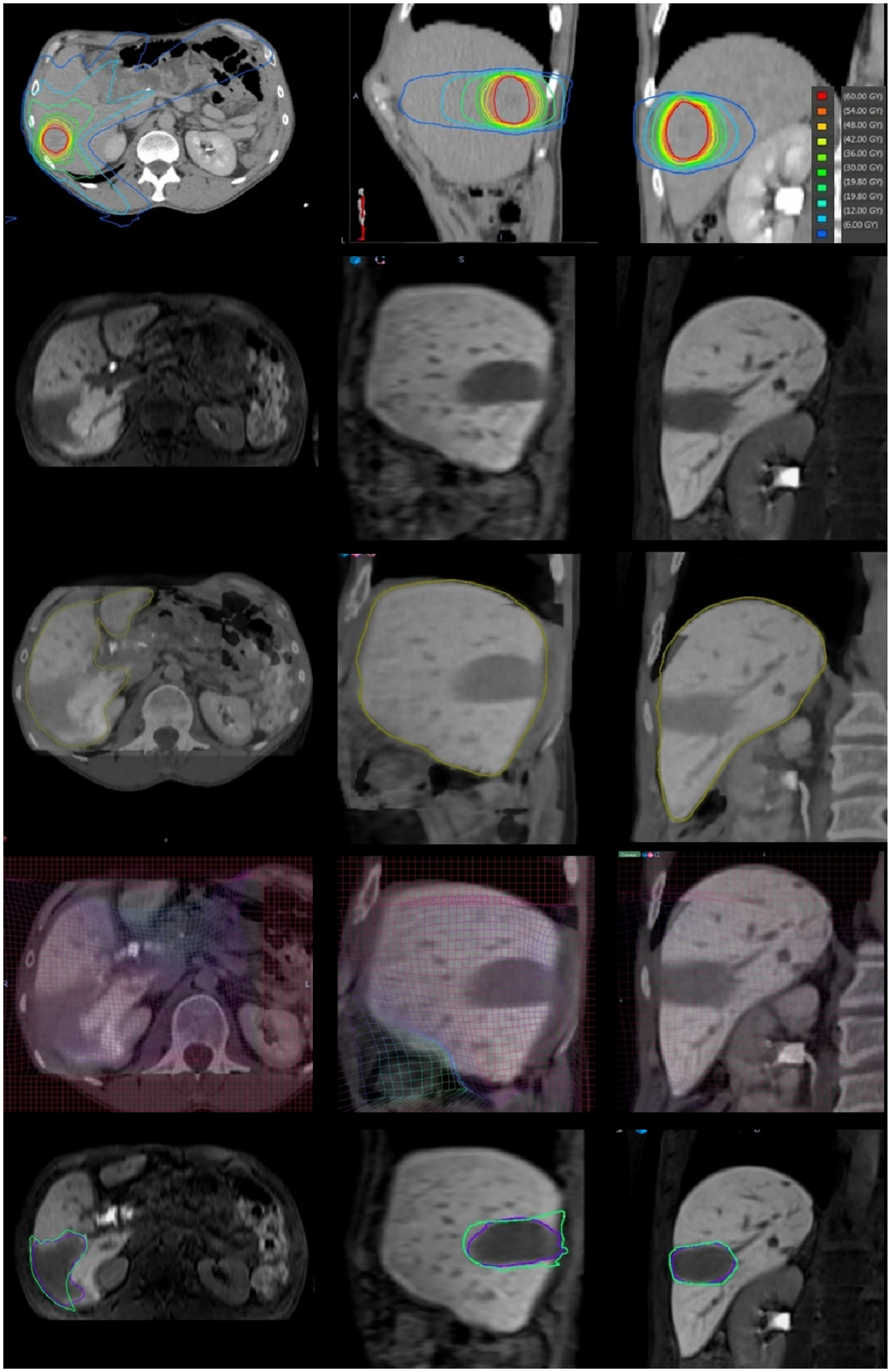

Fig. 1. Patient example of a GS (Gantry-based SBRT). (a) Planning CT with corresponding isodoses, (b–e) post-treatment post-contrast, T1-weighted MRI sequence post-SBRT. (b) Follow-up (FU) MRI with hypo-intense alterations, (c) deformable matching of planning CT with FU-MRI, (d) Displacement grid of the deformable registration, (e) structures (green, isodose line ISL 19.8 Gy cropped to the liver; purple, hypo-intensity/MMA, contoured on non-deformed MRI). (For interpretation of the references to colour in this figure legend, the reader is referred to the web version of this article.)

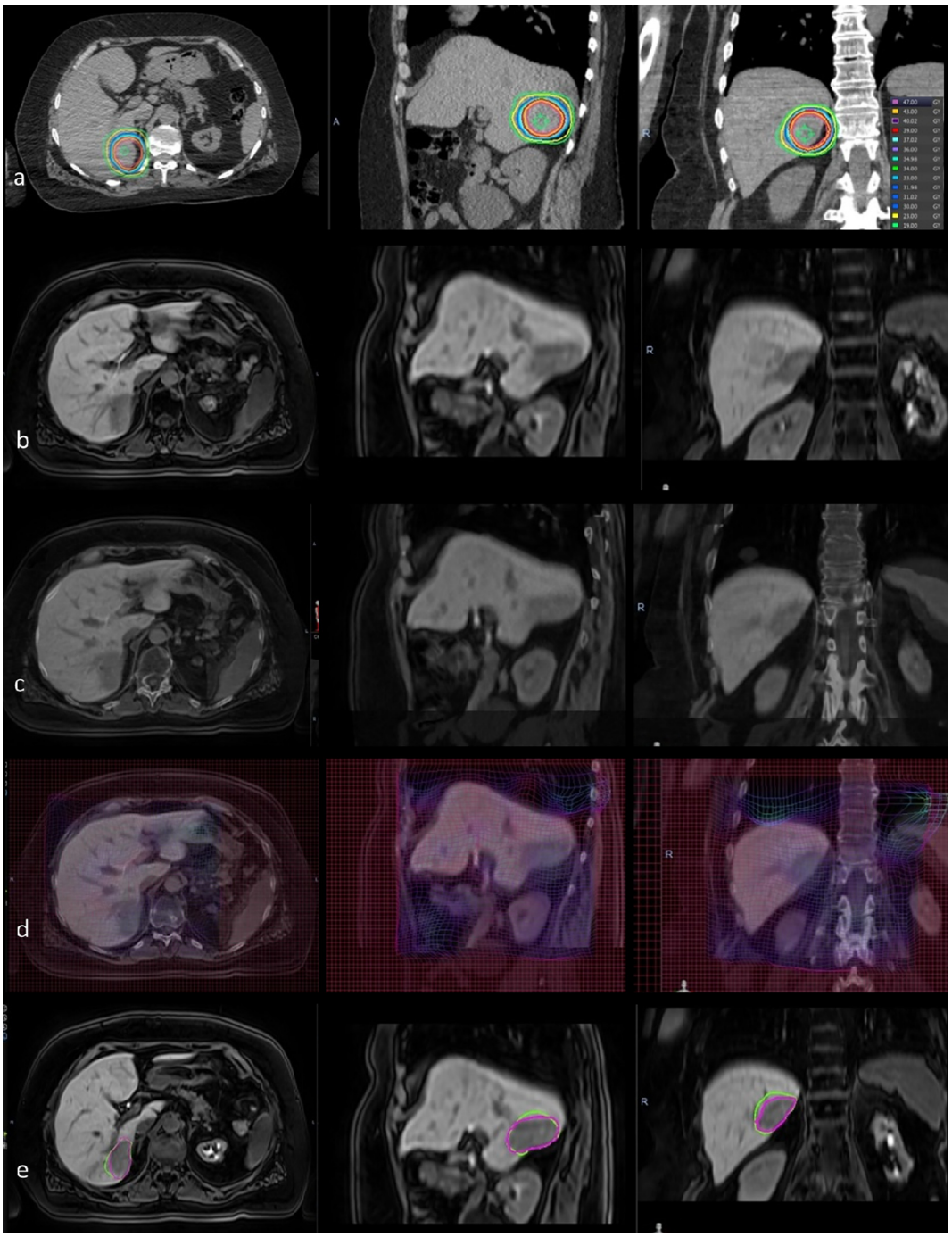

Fig. 2. Patient example of robotic SBRT using the CyberKnife. (a) Planning CT with corresponding isodoses, (b–e) post-treatment post-contrast, T1-weighted MRI sequence post-SBRT. (b) FU MRI with hypo-intense alterations, (c) deformable matching of planning CT with FU MRI, (d) displacement grid of the deformable registration, (e) structures (green, isodose line 31 Gy cropped to the liver/ISL; hypo-intensity/MMA, contoured on non-deformed MRI. (For interpretation of the references to colour in this figure legend, the reader is referred to the web version of this article.)

breath-hold [24], 6–7 breath-hold phases of 15–20 s per CBCT) and dose-delivery were performed during an ABC®-controlled DIBH on a high-end linear accelerator (Versa-HD, Elekta AB) with additional ultrasound-based monitoring of the DIBH-accuracy (Clarity/Anticosti, Elekta AB [21]).

For all RS patients, treatment planning was performed on end-expiration breath-hold CT (1.5 mm slice-thickness) after marker/fiducial implantation in the anatomic proximity of the treated lesions and locoregional matching with the planning MRI. GTV was expanded of 5 mm in the liver and additionally 3 mm isotropically to generate the PTV [1,25]. Median prescription dose was 40 Gy (29–45 Gy) in 3–5 fractions utilizing Sequential Multi-Objective Optimization, with the main objective of reaching GTV mean biological equivalent doses (BED with $\alpha/\beta = 10$ Gy) of $\geq$151.2 Gy_{10} [1,23]. CyberKnife SBRT was delivered with real-time motion compensation (Synchrony®, Accuray Inc.) [1,23,25].

MRT-morphologic alterations (MMA) and corresponding isodose volumes cropped to the liver (ISL)

The treatment planning CT together with the plan dose and contours and the MRI datasets were imported in Velocity™ 3.2.1

(Varian Medical Systems, Palo Alto, Ca, USA) for further processing [10,22]. Post-therapeutic MRI-morphologic alterations (MMA) were contoured and reviewed before image registration by experienced radiation oncologists ($n = 3$), radiologists ($n = 2$) and physicists ($n = 2$) on the T1-weighted, contrast-enhanced (Gd-EOB-DTPA = 35, Gd-DTPA = 2) fast-field-echo (FFE) vibe series of the first follow-up MRI [38] at median 11.5 weeks for RS and 8.8 weeks for GS post-SBRT. MRI acquisition at 1.5 Tesla was performed on various platforms with homogenized post-SBRT imaging protocols. For the DIBH-linac patient cohort, a standardized MRI examination protocol was developed together with the in-house radiology department experts both for therapy planning and regular follow-up. This included fast liver-specific-contrast-enhanced VIBE sequences in DIBH to be easily matched with the planning CT dataset. For the CyberKnife cohort, a similar standardized imaging protocol before and after treatment was used locally at the center, however due to the patient home origins for this center the patients also received imaging at various university hospitals with a similar protocol, though with different vendor MRI systems. For the CyberKnife cohort, all patients received contrast enhanced T1 sequences fully comparable to the other cohort.

The MR-images were registered to the planning-CT and the corresponding dose distributions utilizing structure-based deformable image registration (DIR) software (Velocity 3.2.1) with special attention on the liver ROI. If DIR did not deliver sufficient results by visual control (e.g., due to different breathing phase, inter-current anatomic changes due to surgery or large slice-thickness), loco-regional manual rigid registration was used instead. Registration quality assurance was performed by visual assessment of the tissue/voxel intensity overlay, the deformable warp map (displacement vectors/grid) and display of the difference/displacement map between two registered images.

Based on the image registration the volumetrically and visually best-matching isodose (cropped to the liver, further called ISL) compared to the MMA [10,22] was assigned to the post-SBRT MRI dataset (Figs. 1, 2). Additionally, different isodose lines were tested for the conformity index/DICE coefficient and the one with the highest score has been selected.

In-vivo accuracy (IVA) analysis

For the IVA, the two generated structures (MMA and ISL) were evaluated regarding volume and different geometric parameters in Velocity and for independent validation with Matlab (R2016a, The MathWork Inc, Natick, USA). The difference between the volumes using surface distance metrics (minimum, mean, median, standard deviation, maximum) of the points on one surface to the nearest point on the second structure's surface were calculated to indicate how geometrically close the two structures are. In addition to the surface distance metrics, the conformality index between the two structures was calculated in order to assess the agreement of the ISL to the MMA. The conformality in Velocity is defined as the DICE Coefficient (denoted as conformity index [CI]; range 0–1) of similarity and with that, a measure of structure similarity by comparing overlap and shared volume:

$$CI = (A, B) = \frac{2|A \cap B|}{|A| + |B|}$$

where A is the MMA-volume, B is the ISL-volume and $\cap$ is the overlap volume of the two contours. A CI of 0 means that the structures do not share any volume/overlap in common and a CI of 1 means identical structured regarding volume and overlap.

The number of voxels (%) of each structure outside the other structure was evaluated for assessment of under- and over-coverage of dose to response in order to estimate the homogeneity of the planned dose response in the liver and locate regions of potential local failures. Finally, the center-of-mass difference (CoMD) between MMA and ISL was computed and compared in order to assess the absolute clinical *in-vivo*-accuracy.

Statistical analysis

Parameters influencing IVA were statistically evaluated including influences on conformity, mean and median surface distances, and the 3D-CoMD between MMA and ISL. One-way ANOVA and ANCOVA was performed to investigate the treatment technique factor (RS vs. GS) including GTV mean dose, time to MRI after SBRT, histology (liver primary vs. metastases of colorectal cancer vs. metastases of other primaries), and liver volume reduction as covariates. The statistical analysis was performed with SPSS (version 20.0, IBM, Armonk, NY, USA) and significance was considered at p-value ≤ 0.05.

Results

Liver volume, MRT-morphologic alterations (MMA) and corresponding isodose volumes cropped to the liver (ISL)

A liver volume reduction was observed after RS (−43.1 ± 148.2 cc) and GS (−55.8 ± 174.3 cc) making the registra-

Table 2
Results of IVA analysis after SBRT with advanced motion management techniques (GS and RS). MMA = MRI-morphologic alterations, ISL = MMA corresponding isodose level, DIBH = deep inspiratory breath hold, CoMD = center-of-mass difference, A/P = anterior/posterior, L/R = left/right, S/I = superior/inferior.

	Robotic SBRT (RS) with fiducial tracking *Mean ± SD (Median)*	Gantry-based SBRT (GS) with gating in DIBH *Mean ± SD (Median)*
Liver volume reduction (cc)	−43.1 ± 148.6 (−68.9)	−55.8 ± 174.3 (−22.2)
MMA corresponding ISL (BED, Gy_3)	140.0 ± 42.1 (134.1)	71.6 ± 26.4 (71.1)
MMA volume (cc)	113.0 ± 76.7 (106.5)	166.8 ± 187.0 (109.8)
ISL volume (cc)	118.2 ± 86.5 (111.9)	183.2 ± 198.6 (124.6)
Volume difference *(MMA and ISL, cc)*	5.1 ± 23.3 (3.1)	16.5 ± 34.1 (8.4)
Volume difference *(MMA and ISL, % of ISL)*	1.9 ± 14.4 (3.1)	9.1 ± 15.9 (12.1)
Mean surface distance (mm)	2.3 ± 0.8 (2.2)	2.8 ± 1.1 (2.6)
Maximum Hausdorff surface distance (mm)	27.8 ± 39.2 (15.3)	17.4 ± 9.3 (16.5)
Conformity-Index (CI)	0.83 ± 0.06 (0.83)	0.8 ± 0.07 (0.8)
3D-CoMD *(Velocity, mm)*	3.92 ± 1.97 (3.72)	4.97 ± 2.62 (4.19)
3D-CoMD *(Matlab, mm)*	3.90 ± 1.96 (3.81)	4.98 ± 2.60 (4.18)
Voxel of MMA outside ISL (%)	14.8 ± 7.6 (14.3)	14.8 ± 8.2 (13.3)
ISL to MMA voxel decrease (%)	2.5 ± 11.7 (4.5)	8.7 ± 12.9 (10.7)

Table 3
Statistical analysis using ANOVA and ANCOVA. MMA = MRI-morphologic alterations, ISL = to MMA corresponding isodose level, CoMD = center-of-mass difference, GTV = gross tumor volume, PTV = planning target volume, BED = biological equivalent dose, EQD2 = equivalent dose in 2 Gy fractions.

Parameter (co-variate)	Conformity-Index (CI) *(MMV and ISL)*	Mean surface distance *(MMV and ISL, mm)*	3D-CoMD *(MMV and ISL, mm)*
Histology	0.265	0.483	0.267
GTV	0.041*	0.468	0.605
PTV	0.020*	0.557	0.753
PTV prescription BED	0.170	0.061	0.146
GTV mean BED	0.254	0.329	0.417
Prior chemotherapy	0.377	0.313	0.657
Prior radiotherapy	0.989	0.114	0.158
Whole liver volume	0.784	0.721	0.589
Whole liver EQD2	0.074	0.390	0.908
Normal liver volume	0.198	0.989	0.410
Normal liver EQD2	0.170	0.259	0.657
MRI slice thickness	0.690	0.089	0.550
Technique	0.112	0.290	0.086
Technique (histology)	0.016* (0.022)	0.038* (0.283)	0.245 (0.292)
Technique (GTV mean BED)	0.160 (0.379)	0.120 (0.489)	0.205 (0.568)
Technique (time SBRT to MRI)	0.103 (0.631)	0.088 (0.701)	0.181 (0.863)
Technique (liver volume reduction)	0.121 (0.345)	0.093 (0.211)	0.171 (0.568)

*p-values, statistically significant.

tion of the datasets (in addition to diverging breathing phases of CT and MRI datasets) difficult for some series for the full liver volume (Table 2). For RS the MMA of all cases was hypo-intense and for GS the MMA was hyper-intense in eight and hypo-intense in twelve cases on the post-contrast T1-weighted MRI, similarly to previously published observations [10,22]. The volume of the MMA was 113.0 ± 76.8 cc (median 106.5 cc) for RS and 166.8 ± 187.8 cc (median 109.8 cc) for GS. The corresponding isodose BED ($\alpha/\beta = 3$ for healthy liver-tissue) was 140.0 ± 42.1 Gy_3 (median 134.1 Gy_3) for RS and 71.6 ± 26.4 Gy_3 (median 71.1 Gy_3) for GS, respectively. The volume of best fitting ISL was 118.2 ± 86.5 cc (median 111.9 cc) for RS and 183.2 ± 198.6 cc (median 124.6 cc) for GS. ISL- and MMA volumes diverged by 5.1 ± 23.3 cc (RS) and 16.5 ± 34.1 cc (GS, Table 2).

In-vivo accuracy (IVA) analysis

The mean of the mean surface distance of MMA and ISL was 2.3 ± 0.8 mm (RS) and 2.8 ± 1.0 mm (GS). The median CI of both structures was 0.83 (range 0.60–0.91) for RS and 0.80 (range 0.69–0.91) for GS, respectively. The Matlab-computed median absolute 3D-CoMD was 3.8 mm (range 0.9–7.5 mm) for RS and 4.2 mm (range 1.5–9.8 mm) for GS. The mean of the relative directional errors were all well below 1 mm but for the left–right direction for RS (1.1 mm) and the standard deviation of the mean errors were below 3 mm but for the anterior-posterior direction for GS (4.1 mm). A median of 14.3% and 14.8% of all voxels of the MMA were outside ISL and a median of 14.8% and 23.5% of all voxels of the ISL were outside MMA for RS and GS, respectively. The median voxel decrease from ISL to MMA was 4.5% for RS and 10.7% for GS (Table 2).

Factors influencing IVA

IVA as evaluated by CI, mean and median surface distances and 3D-CoMD between MMA and ISL had no significant dependence on the treatment technique in the ANOVA (Table 3). Not surprisingly, however, the GTV and PTV significantly influenced the CI ($p = 0.041$ and $p = 0.020$) as larger volumes with similar overlap have a higher CI as a consequence of the definition of the index. Otherwise, no parameter such as histology, prescriptions or mean dose, prior treatment, liver volume and dose or MRI slice thickness influenced the IVA. The non-significant dependence of the IVA based on the technique also did not change after adjusting for post-treatment changes of liver volume, mean GTV dose or the time from SBRT to MRI in the ANCOVA. However, using histology as co-variate, the CI and the mean surface distance between the MMA and ISL were significantly associated with the treatment technique ($p = 0.016$ and $p = 0.038$). This basically translates into a high average CI for primary liver tumors (0.89), a medium average CI for colorectal metastases (0.80) and a low average CI for other histology metastases (0.77) for GS, which again is not surprising when looking at the tumor volumes and the ANOVA in detail.

Clinical results

During follow-up, (range 3.6–74.5 months, median 13.6 months) one local recurrence (LR) was found for GS (time to LR = 26.7 months, CoMD = 6.0 mm) and three LR were found for RS (time to LR = 38.5/20.7/9.7 months, CoMD = 1.9/2.2/5.2 mm). Based on a geometric sub-analysis we were not able to correlate the center-of-mass shift between ISL and MMA to the location of the LR. To the contrary, for the third LR 9.7 months after RS (CoMD = 5.2 mm) the MMA shift was in the direction of the LR. Therefore, the reason for the LR was based on other factors than treatment accuracy, likely being dose for GS (PTV overlap with the colon) or loco-regional tumor spread for all three RS LR as this is not uncommon for colorectal liver metastases [26].

Discussion

For liver tumors, precise stereotactic body radiotherapy (SBRT) delivery with advanced motion management techniques can have a impact on treatment success regarding local control and toxicity as a large multi-center analysis has recently demonstrated [2]. Post-SBRT imaging with radiation-induced changes in the healthy liver tissue surrounding the gross tumor volume (GTV) can already visually prove, that high doses being used in SBRT were applied correctly. However, to our best knowledge, *in-vivo* quantification of the treatment delivery precision for liver SBRT has never been performed before.

The method, which we introduced to our best knowledge, the first time in the literature, is a novel approach to provide detailed *in-vivo* accuracy information after SBRT treatments in the liver using dose-to-outcome registration based on follow-up imaging. Recently, the question of the IVA has also been investigated by Jung

et al. [27] where the authors analyzed post-SBRT changes for 29 HCC patients. They found a 3D-accuracy of their method of 5.60 mm (diaphragm guidance) and 7.53 mm (marker guidance), which came as a surprise as diaphragm guidance had been considered to be less accurate for liver SBRT compared to direct tumor or surrogate guidance [28,29]. Further noteworthy, their MRI-morphologic alterations (MMA) at follow-up were not compared to the treatment plan and the corresponding isodoses, but only to the center of the HCC on the same follow-up MRI. Hence, no real accuracy information could be drawn from that work as numerous rather inaccurate assumptions were made for the actual treatment technique. This shortcoming was overcome by our method as we compared the intended treatment plan and isodose distribution with the consequent MMA linking plan and outcome with each other based on deformable registration and structure analysis.

In fact, when comparing the corresponding ISL with the MMA we found low median volume decreases between ISL and MMA of 4.5% (RS) and 10.7% (GS). Surely, variations in overall liver tissue dose–response and post-SBRT variable time-to-MRI were compensated for using a best-match-concept for the ISL, but still, the overall geometric dose calculation accuracy of both methods appears to be striking despite the different residual delivery inaccuracies of both methods [21,30,31] and the likelihood of non-homogeneous liver tissue responses. Another explanation for the MMA volume decrease compared to the ISL may be the observed liver volume decreases after SBRT that appear to be similar to the post-hemihepatectomy situation. The initial liver volume decrease may however likely be reversed during later follow-up while the MMA may disappear completely when the liver heals [32,33].

For the IVA of our active motion compensation techniques we found mean surface distances of the ISL and MMA of <3 mm. The median conformity index (CI) of both structures was >0.80 for both GS and RS and the median 3D center-of-mass difference (CoMD) of ISL and MMA was 4.2 mm for GS and 3.7 mm for RS without any trace of systematic errors and well in agreement with technical accuracy studies published previously [20,25,34–38]. We can therefore safely assume that the overall treatment accuracy of advanced active motion management with deep inspiration breath-hold gating including ultrasound validation and fiducial-based real-time robotic tracking is below 5 mm and that random error components can be compensated for by a 5 mm PTV-margin accordingly. Factors influencing the IVA were gross tumor and planning target volume and histology, though only on the conformity of ISL and MMA by definition of the CI and likely due to changing liver deformability due to cirrhosis for HCC patients. On the other hand, the 3D-CoMD was not influenced by any treatment factor, including treatment technique, pointing once more at the existence of random but not systematic residual error components for RS and GS liver SBRT. However, if no advanced motion management methods are used (e.g. ITV concepts with 4DCT and/or motion-compression), a likelihood of higher treatment inaccuracy must be assumed and further research about these methods is needed and underway.

There are, of course, potential sources of error of the presented method, which should be considered for the final interpretation of these results. Volume changes of the tumor and/or the liver due to post-SBRT regeneration can influence the quality of the deformable registration. Heterogeneity in time-to-MRI, imaging protocols and image resolution, especially slice thickness, will influence the resolution of the accuracy estimation. Yet regardless of heterogeneous (RS) or homogenous (GS) MRI image resolution/protocols, the results in both cohorts are comparable and not statistically influenced by those factors. The results can additionally be influenced by registrations errors [39,40] and inter-user contouring differences. However, due to involvement of several centers and multiple independent experts, we assume that this source of error was minimized in our presented analysis.

A further possible source of inaccuracy could be introduced during the planning procedure (matching of planning CT with the planning MRI). Robotic SBRT plans were created primarily on contrast-enhanced CT imaging and implanted fiducial markers. The exhale MRI was loco-regionally registered to the tumor region. This uncertainty however is included in the overall accuracy of the whole delivery chain, since we specifically compared the static dose to the actual *in-vivo* response and we demonstrated quite high agreements between the shape of the isodose and the MMA, despite all uncertainties given during treatment. Hence, we believe that the impact on liver deformation or residual uncertainties during treatment with the CyberKnife appears to be low. The same is true for residual motion during DIBH gated delivery which we demonstrated as well. There are residual uncertainties for both methods. Residual error of the ABC-based gating is a known phenomenon (baseline shift which can be corrected by daily image-guided repositioning and inter- and intra-breath hold uncertainties which can/should be compensated with the PTV margins). In our paper published in the Journal this year [21] we reported a residual superior-inferior error of less than 5 mm in 95% of the cases based on ultrasound-based online monitoring of the breath-holds. The IVA analysis mirrors this situation and for some cases, where lower IVA was observed, a delivery miss can be suspected in some fractions.

In summary, both techniques have impressively shown median deviations <5 mm of the planned isodoses cropped to the liver and matched to the MRI-morphologic alterations observed during first follow-up. Furthermore, the IVA has also shown a few patients with larger errors than 5 mm, clearly raising again the question for patient-specific safety margins for the dose application during motion-compensated SBRT [21,25]. Yet the clinical outcome analysis revealed no correlation between local recurrence and *in-vivo* accuracy at the levels observed in this analysis. Hence, other factors (e.g. lower prescription, mean or maximum dose [4] or microscopic loco-regional lesion recurrence [26] may be alternative explanations for local treatment failure and may have a higher influence on treatment success than the minimal inaccuracies of motion-compensated dose application with GS/RS SBRT.

For the first time, a method for dosimetric *in-vivo* accuracy assessment for motion compensated liver stereotactic body radiotherapy with gantry-based gating and robotic-based tracking delivery is presented. The observed data can serve as a benchmark for other application techniques. Potential sources of error (e.g. volume changes of the tumor and/or liver, temporal/biologic modelling of *in-vivo* reaction of healthy tissue to the delivered dose, image resolution, registration errors, inter-user contouring differences) have to be considered and may potentially limit the quality of the results, but both techniques have impressively shown median deviations <5 mm from the planned isodoses to the MRI-morphologic alterations noticed during first follow-up.

Conflicts of interest

FW reports institutional grants unrelated to the study from Elekta AB, Sweden, during the time the study was conducted. All other authors report no conflicts of interest.

References

[1] Andratschke N, Parys A, Stadtfeld S, Wurster S, Huttenlocher S, Imhoff D, et al. Clinical results of mean GTV dose optimized robotic guided SBRT for liver metastases. Radiat Oncol 2016;11:74. https://doi.org/10.1186/s13014-016-0652-4.

[2] Andratschke N, Alheid H, Allgauer M, Becker G, Blanck O, Boda-Heggemann J, et al. The SBRT database initiative of the German Society for Radiation Oncology (DEGRO): patterns of care and outcome analysis of stereotactic body radiotherapy (SBRT) for liver oligometastases in 474 patients with 623 metastases. BMC Cancer 2018;18:283. https://doi.org/10.1186/s12885-018-4191-2.

[3] Mahadevan A, Blanck O, Lanciano R, Peddada A, Sundararaman S, D'Ambrosio D, et al. Stereotactic Body Radiotherapy (SBRT) for liver metastasis - clinical outcomes from the international multi-institutional RSSearch(R) Patient Registry. Radiat Oncol 2018;13:26. https://doi.org/10.1186/s13014-018-0969-2.

[4] Klement RJ, Guckenberger M, Alheid H, Allgauer M, Becker G, Blanck O, et al. Stereotactic body radiotherapy for oligo-metastatic liver disease - Influence of pre-treatment chemotherapy and histology on local tumor control. Radiother Oncol 2017;123:227–33. https://doi.org/10.1016/j.radonc.2017.01.013.

[5] Boda-Heggemann J, Dinter D, Weiss C, Frauenfeld A, Siebenlist K, Attenberger U, et al. Hypofractionated image-guided breath-hold SABR (stereotactic ablative body radiotherapy) of liver metastases–clinical results. Radiat Oncol 2012;7:92. https://doi.org/10.1186/1748-717X-7-92.

[6] Sterzing F, Brunner TB, Ernst I, Baus WW, Greve B, Herfarth K, et al. Stereotactic body radiotherapy for liver tumors: principles and practical guidelines of the DEGRO Working Group on Stereotactic Radiotherapy. Strahlenther Onkol 2014;190:872–81. https://doi.org/10.1007/s00066-014-0714-1.

[7] Olsen CC, Welsh J, Kavanagh BD, Franklin W, McCarter M, Cardenes HR, et al. Microscopic and macroscopic tumor and parenchymal effects of liver stereotactic body radiotherapy. Int J Radiat Oncol Biol Phys 2009;73:1414–24. https://doi.org/10.1016/j.ijrobp.2008.07.032.

[8] Herfarth KK, Hof H, Bahner ML, Lohr F, Hoss A, van Kaick G, et al. Assessment of focal liver reaction by multiphasic CT after stereotactic single-dose radiotherapy of liver tumors. Int J Radiat Oncol Biol Phys 2003;57:444–51.

[9] Howells CC, Stinauer MA, Diot Q, Westerly DC, Schefter TE, Kavanagh BD, et al. Normal liver tissue density dose response in patients treated with stereotactic body radiation therapy for liver metastases. Int J Radiat Oncol Biol Phys 2012;84:e441–446. https://doi.org/10.1016/j.ijrobp.2012.04.041.

[10] Boda-Heggemann J, Jahnke A, Chan MKH, Ghaderi Ardekani LS, Hunold P, Schafer JP, et al. Direct dose correlation of MRI morphologic alterations of healthy liver tissue after robotic liver SBRT. Strahlenther Onkol 2018;194:414–24. https://doi.org/10.1007/s00066-018-1271-9.

[11] El Naqa I, Johansson A, Owen D, Cuneo K, Cao Y, Matuszak M, et al. Modeling of normal tissue complications using imaging and biomarkers after radiation therapy for hepatocellular carcinoma. Int J Radiat Oncol Biol Phys 2018;100:335–43. https://doi.org/10.1016/j.ijrobp.2017.10.005.

[12] Fukugawa Y, Namimoto T, Toya R, Saito T, Yuki H, Matsuyama T, et al. Radiation-induced liver injury after 3D-conformal radiotherapy for hepatocellular carcinoma: quantitative assessment using Gd-EOB-DTPA-enhanced MRI. Acta Med Okayama 2017;71:25–9. https://doi.org/10.18926/AMO/54822.

[13] Kellock T, Liang T, Harris A, Schellenberg D, Ma R, Ho S, et al. Stereotactic body radiation therapy (SBRT) for hepatocellular carcinoma: imaging evaluation post treatment. Br J Radiol 2018;91:20170118. https://doi.org/10.1259/bjr.20170118.

[14] Mendiratta-Lala M, Gu E, Owen D, Cuneo KC, Bazzi L, Lawrence TS, et al. Imaging findings within the first 12 months of hepatocellular carcinoma treated with stereotactic body radiation therapy. Int J Radiat Oncol Biol Phys 2017. https://doi.org/10.1016/j.ijrobp.2017.08.022.

[15] Dreher C, Hoyer KI, Fode MM, Habermehl D, Combs SE, Hoyer M. Metabolic liver function after stereotactic body radiation therapy for hepatocellular carcinoma. Acta Oncol 2016;55:886–91. https://doi.org/10.3109/0284186X.2015.1137352.

[16] Barry A, McPartlin A, Lindsay P, Wang L, Brierley J, Kim J, et al. Dosimetric analysis of liver toxicity after liver metastasis stereotactic body radiation therapy. Pract Radiat Oncol 2017;7:e331–7. https://doi.org/10.1016/j.prro.2017.03.004.

[17] Su TS, Luo R, Liang P, Cheng T, Zhou Y, Huang Y. A prospective cohort study of hepatic toxicity after stereotactic body radiation therapy for hepatocellular carcinoma. Radiother Oncol 2018;129(1):136–142. https://doi.org/10.1016/j.radonc.2018.02.031.

[18] Gkika E, Bettinger D, Krafft L, Schultheiss M, Neeff HP, Maruschke L, et al. The role of albumin-bilirubin grade and inflammation-based index in patients with hepatocellular carcinoma treated with stereotactic body radiotherapy. Strahlenther Onkol 2018;194:403–13. https://doi.org/10.1007/s00066-017-1256-0.

[19] Nabavizadeh N, Waller JG, Fain 3rd R, Chen Y, Degnin CR, Elliott DA, et al. Safety and efficacy of accelerated hypofractionation and stereotactic body radiation therapy for hepatocellular carcinoma patients with varying degrees of hepatic impairment. Int J Radiat Oncol Biol Phys 2018;100:577–85. https://doi.org/10.1016/j.ijrobp.2017.11.030.

[20] Sihono DS, Vogel L, Weiss C, Tholking J, Wenz F, Lohr F, et al. A 4D ultrasound real-time tracking system for external beam radiotherapy of upper abdominal lesions under breath-hold. Strahlenther Onkol 2017;193:213–20. https://doi.org/10.1007/s00066-016-1076-7.

[21] Vogel L, Sihono DSK, Weiss C, Lohr F, Stieler F, Wertz H, et al. Intra-breath-hold residual motion of image-guided DIBH liver-SBRT: an estimation by ultrasound-based monitoring correlated with diaphragm position in CBCT. Radiother Oncol 2018;129(3):441–8. https://doi.org/10.1016/j.radonc.2018.07.007.

[22] Boda-Heggemann J, Attenberger U, Budjan J, Jahnke A, Jahnke L, Vogel L, et al. MRI morphologic alterations after liver SBRT: Direct dose correlation with intermodal matching. Strahlenther Onkol 2016;192:641–8. https://doi.org/10.1007/s00066-016-1013-9.

[23] Stera S, Balermpas P, Chan MKH, Huttenlocher S, Wurster S, Keller C, et al. Breathing-motion-compensated robotic guided stereotactic body radiation therapy: Patterns of failure analysis. Strahlenther Onkol 2018;194:143–55. https://doi.org/10.1007/s00066-017-1204-z.

[24] Boda-Heggemann J, Knopf AC, Simeonova-Chergou A, Wertz H, Stieler F, Jahnke A, et al. Deep inspiration breath hold-based radiation therapy: a clinical review. Int J Radiat Oncol Biol Phys 2016;94:478–92. https://doi.org/10.1016/j.ijrobp.2015.11.049.

[25] Chan M, Grehn M, Cremers F, Siebert FA, Wurster S, Huttenlocher S, et al. Dosimetric implications of residual tracking errors during robotic SBRT of liver metastases. Int J Radiat Oncol Biol Phys 2017;97:839–48. https://doi.org/10.1016/j.ijrobp.2016.11.041.

[26] Mendez Romero A, Verheij J, Dwarkasing RS, Seppenwoolde Y, Redekop WK, Zondervan PE, et al. Comparison of macroscopic pathology measurements with magnetic resonance imaging and assessment of microscopic pathology extension for colorectal liver metastases. Int J Radiat Oncol Biol Phys 2012;82:159–66. https://doi.org/10.1016/j.ijrobp.2010.10.032.

[27] Jung J, Kim H, Yoon SM, Cho B, Kim YJ, Kwak J, et al. Targeting accuracy of image-guided stereotactic body radiation therapy for hepatocellular carcinoma in real-life clinical practice. in vivo assessment using hepatic parenchymal changes on Gd-EOB-DTPA-enhanced magnetic resonance images. Int J Radiat Oncol Biol Phys. 2018. https://doi.org/10.1016/j.ijrobp.2018.05.018.

[28] Chan MK, Lee V, Chiang CL, Lee FA, Law G, Sin NY, et al. Lipiodol versus diaphragm in 4D-CBCT-guided stereotactic radiotherapy of hepatocellular carcinomas. Strahlenther Onkol 2016;192:92–101. https://doi.org/10.1007/s00066-015-0929-9.

[29] Heinz C, Gerum S, Freislederer P, Ganswindt U, Roeder F, Corradini S, et al. Feasibility study on image guided patient positioning for stereotactic body radiation therapy of liver malignancies guided by liver motion. Radiat Oncol 2016;11:88. https://doi.org/10.1186/s13014-016-0662-2.

[30] Josipovic M, Persson GF, Bangsgaard JP, Specht L, Aznar MC. Deep inspiration breath-hold radiotherapy for lung cancer: impact on image quality and registration uncertainty in cone beam CT image guidance. Br J Radiol 2016;89:20160544. https://doi.org/10.1259/bjr.20160544.

[31] Kashani R, Balter JM, Hayman JA, Henning GT, van Herk M. Short-term and long-term reproducibility of lung tumor position using active breathing control (ABC). Int J Radiat Oncol Biol Phys 2006;65:1553–9. https://doi.org/10.1016/j.ijrobp.2006.04.027.

[32] Farach A, Quesada J, Teh BS. Liver regeneration following repeat SBRT. J Gastrointest Oncol 2015;6:E2–6. https://doi.org/10.3978/j.issn.2078-6891.2014.082.

[33] Theysohn JM, Ertle J, Muller S, Schlaak JF, Nensa F, Sipilae S, et al. Hepatic volume changes after lobar selective internal radiation therapy (SIRT) of hepatocellular carcinoma. Clin Radiol 2014;69:172–8. https://doi.org/10.1016/j.crad.2013.09.009.

[34] Blessing M, Hofmann J, Vogel L, Boda-Heggemann J, Lohr F, Wenz F, et al. An offline technique to evaluate residual motion of the diaphragm during deep inspiratory breath-hold from cone-beam CT datasets. Strahlenther Onkol 2018. https://doi.org/10.1007/s00066-018-1313-3.

[35] Simeonova-Chergou A, Jahnke A, Siebenlist K, Stieler F, Mai S, Boda-Heggemann J, et al. Automatically gated image-guided breath-hold IMRT is a fast, precise, and dosimetrically robust treatment for lung cancer patients. Strahlenther Onkol 2016;192:166–73. https://doi.org/10.1007/s00066-015-0934-z.

[36] Nankali S, Worm ES, Hansen R, Weber B, Hoyer M, Zirak A, et al. Geometric and dosimetric comparison of four intrafraction motion adaptation strategies for stereotactic liver radiotherapy. Phys Med Biol 2018;63:. https://doi.org/10.1088/1361-6560/aacdda145010.

[37] Sothmann T, Blanck O, Poels K, Werner R, Gauer T. Real time tracking in liver SBRT: comparison of CyberKnife and Vero by planning structure-based gamma-evaluation and dose-area-histograms. Phys Med Biol 2016;61:1677–91. https://doi.org/10.1088/0031-9155/61/4/1677.

[38] Winter JD, Wong R, Swaminath A, Chow T. Accuracy of robotic radiosurgical liver treatment throughout the respiratory cycle. Int J Radiat Oncol Biol Phys 2015;93:916–24. https://doi.org/10.1016/j.ijrobp.2015.08.031.

[39] Latifi K, Caudell J, Zhang G, Hunt D, Moros EG, Feygelman V. Practical quantification of image registration accuracy following the AAPM TG-132 report framework. J Appl Clin Med Phys 2018;19:125–33. https://doi.org/10.1002/acm2.12348.

[40] Zhang L, Wang Z, Shi C, Long T, Xu XG. The impact of robustness of deformable image registration on contour propagation and dose accumulation for head and neck adaptive radiotherapy. J Appl Clin Med Phys 2018;19:185–94. https://doi.org/10.1002/acm2.12361.